Hindawi
Mathematical Problems in Engineering
Volume 2018, Article ID 8767895, 9 pages
https://doi.org/10.1155/2018/8767895

Research Article

The Influence of Pits on the Tribological Behavior of Grey Cast Iron under Dry Sliding

Risheng Long,[1,2,3] **Peter Kelly**,[4] **Shaoni Sun**,[5] **Jiling Feng**,[4] **Xuewen Wang**,[2,3] **and Wenyue Li**[2,3]

[1]*College of Mechanical Engineering, Shenyang University of Chemical Technology, Shenyang, Liaoning 110142, China*
[2]*College of Mechanical Engineering, Taiyuan University of Technology, Taiyuan, Shanxi 030024, China*
[3]*Shanxi Key Laboratory of Fully Mechanized Coal Mining Equipment, Taiyuan, Shanxi 030024, China*
[4]*Surface Engineering Group, Manchester Metropolitan University, Manchester M1 5GD, Lancs, UK*
[5]*School of Mechanical Engineering and Automation, Northeastern University, Shenyang, Liaoning 110819, China*

Correspondence should be addressed to Peter Kelly; peter.kelly@mmu.ac.uk

Received 1 April 2018; Revised 25 June 2018; Accepted 19 July 2018; Published 27 August 2018

Academic Editor: Matteo Aureli

Inspired by the nonsmooth surface of the head of the dung beetle, grey cast iron (GCI) samples with pit textured surfaces were designed and fabricated, based on pin-on-disc friction tester. Using a tribology wear testing rig and APDL programming, the tribological behavior of smooth and textured samples was investigated and reported, both experimentally and numerically. The results show that pits can significantly change the thermal stress and temperature distribution on the surface, which will result in either positive or negative effects on the wear resistance of GCI samples, depending on the parameters. When diameter of the pit (DOP) equals 0.8 mm and distance between pits (DBP) is 1.0 mm, the pit textured surface provided the best wear resistance among all samples tested.

1. Introduction

Grey cast iron (GCI) is one of the most commonly used materials in industrial applications, including, for example, the base and guideways of machine tools, cylinder block of automobile engine, bodies of valves and pumps, reduction gear shells, and trains brake discs, owing to its high friction coefficient, low cost, good damping property, and fine castability and machinability, as well as other properties [1]. For any mechanical system, the relative movement of different parts in contact is inevitable, such as the guideway of a lathe and the bearing mounting position of a gearbox, wherein friction and wear can only be reduced, instead of eliminated or avoided, especially under dry sliding conditions. Therefore, to meet the higher demand for accuracy, speed, and reliability of future applications, like the heavy-duty braking systems of high-speed trains, it is of great significance and urgency to further improve and enhance the wear resistance of GCI parts.

Surface texturing (ST) and biomimetic nonsmooth surfaces (BNSS) provide us two choices from different viewpoints. ST, firstly presented by Hamilton et al. in 1966, is a means for enhancing the tribological performance of mechanical components, through material-removal methods, like electrical discharge machining (EDM), industrial etching/chemical milling, laser surface texturing (LST), or other techniques [2–4]. BNSS was proposed and developed by Ren et al. in Jilin University since the 1980s and is inspired by the unique functional surfaces of natural animals (see Figure 1) and plants, which have gradually developed to best adapt to different environments, through billions of years of natural selection and evolution [5]. Those surface structures (pits, streaks, and rectangles), called 'nonsmooth construction units', are mainly obtained by material remelting/cladding techniques and can provide excellent wear resistance, fatigue resistance, and crack resistance [6, 7].

In the past years, great efforts have been made to study the influence of different nonsmooth surfaces on the thermal

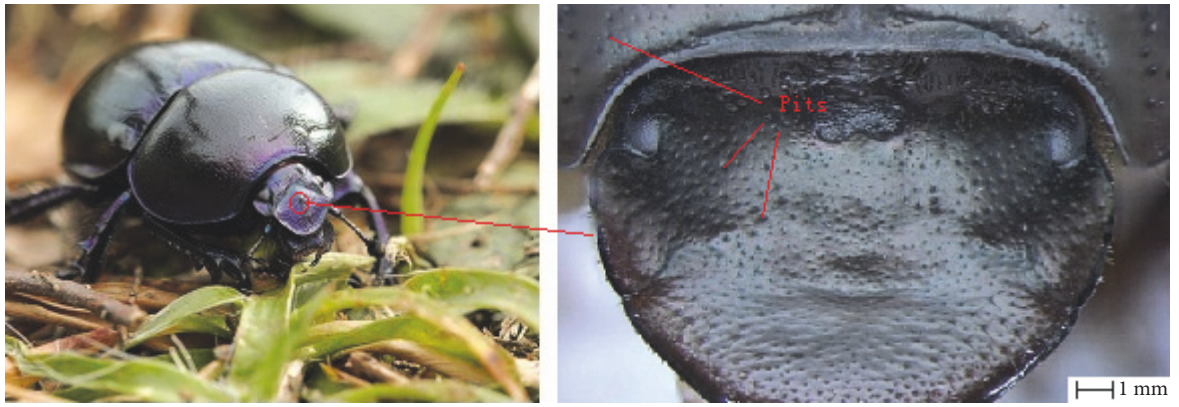

Figure 1: Dung beetle and the pit nonsmooth surface of its head.

fatigue resistance of GCI parts [1, 8–14]. In contrast, studies of the antiwear performance or tribological behavior of GCI parts with textured surfaces are quite few, whether in experiment or simulation, especially under dry wear conditions. Based on the previous research on the thermal behavior of pin-on-disc friction systems [15, 16], a finite element model with linearly distributed pits in the radial direction (LDRD) was first established through APDL (ANSYS parametric design language) programming. The influence of different pit parameters on the tribological behavior was researched. The friction coefficient curves and mass losses of samples were measured and reported. The worn surfaces were characterized by stereo-optical microscope. All the obtained data could provide an important reference for the design of heavy-duty braking system, rotating thrust bearing, heavy-load sliding bearing, and so on.

2. Modelling and Testing Procedure

2.1. Thermodynamics Theory and Conditions. For certain conditions, the heat conduction during friction processes can be described by the classical heat conduction equation. In the Cartesian coordinate system, the classical heat conduction equation can be expressed as follows [16]:

$$k_e\left(\frac{\partial^2 T}{\partial x^2}+\frac{\partial^2 T}{\partial y^2}+\frac{\partial^2 T}{\partial z^2}\right)+q+h\left(T-T_h\right)+\sigma\varepsilon\left(T^4-T_h^4\right)=\rho\cdot c\frac{\partial T}{\partial t} \tag{1}$$

where k_e is the thermal conductivity of material, c is the specific heat capacity of material, q is the heat flux through the contact area, ρ is the density of material, h is the convective heat transfer coefficient, T_h is the ambient temperature, σ is the radiation constant of a blackbody, and ε is the radiation rate of the actual object.

To solve (1), the initial condition and boundary conditions are necessary. In this work, the initial condition is the original temperature of the pin-on-disc system at the beginning of the simulation, equal to 20°C. The boundary condition is the heat exchange condition between the outer surface of the pin-on-disc system and its surrounding environment [15].

The heat flux, q_w, at the boundary of the objects, is a known constant or also a function of position and time. For pin-on-disc friction systems, it can be expressed as

$$-k\left(T\right)\left.\frac{\partial T}{\partial \vec{n}}\right|_s=q_w \quad \text{or} \quad -k\left(T\right)\left.\frac{\partial T}{\partial \vec{n}}\right|_s=q_w\left(x,y,z,t\right) \tag{2}$$

$$q_w\left(x,y,z,t\right)=\eta\cdot\mu\cdot P\cdot v\left(x,y,z,t\right) \tag{3}$$

where q_w is the heat flux through the contact surface of the pin-on-disc system, a known constant; $q_w(x, y, z, t)$ is the expression of input heat flux, a function of position and time; η is the conversion efficiency, 0.85; μ is the friction coefficient of the system, 0.38; P is the normal pressure of the pin; $v(x, y, z, t)$ is the relative linear velocity between disc and pin. Meanwhile, the lower surface of the disc can be regarded as being in the adiabatic state, whose boundary condition can be written as

$$-k_e\frac{\partial T}{\partial z}=0 \tag{4}$$

For pin-on-disc friction systems, the temperature distribution in the disc or the pin is very uneven during dry wear processes. As a result, a huge temperature gradient exists in the disc, which further induces high thermal stresses. Thus, the thermal strain is composed of two parts: one is caused by temperature variation, and the other is caused by stress. According to Hooke's law, the thermal strain can be written as

$$\varepsilon_{xx}=\frac{\partial u_x}{\partial x}=\frac{1}{E}\left[\sigma_{xx}-\nu\left(\sigma_{yy}+\sigma_{zz}\right)\right]+\alpha\tau=\frac{1}{2G}\left(\sigma_{xx}-\frac{\nu}{1+\nu}\Theta_s\right)+\alpha\tau$$

$$\varepsilon_{yy}=\frac{\partial u_y}{\partial y}=\frac{1}{E}\left[\sigma_{yy}-\nu\left(\sigma_{xx}+\sigma_{zz}\right)\right]+\alpha\tau$$

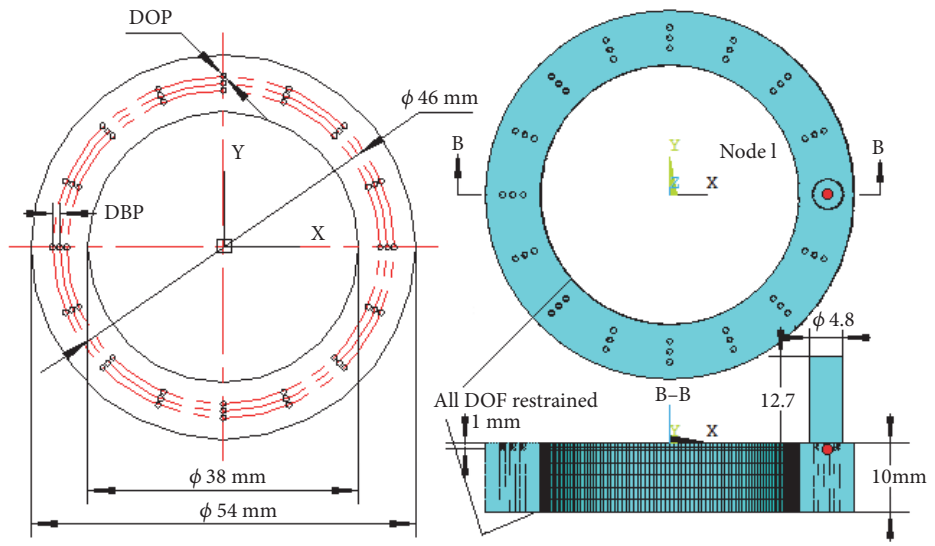

Figure 2: The finite element model with pit textured surface and the location of node 1.

$$= \frac{1}{2G}\left(\sigma_{yy} - \frac{\nu}{1+\nu}\Theta_s\right) + \alpha\tau$$

$$\varepsilon_{zz} = \frac{\partial u_z}{\partial z} = \frac{1}{E}\left[\sigma_{zz} - \nu\left(\sigma_{xx} + \sigma_{yy}\right)\right] + \alpha\tau$$

$$= \frac{1}{2G}\left(\sigma_{zz} - \frac{\nu}{1+\nu}\Theta_s\right) + \alpha\tau$$

$$\Theta_s = \sigma_{xx} + \sigma_{yy} + \sigma_{zz},$$

$$\varepsilon_{xy} = \frac{\sigma_{xy}}{2G},$$

$$\varepsilon_{yz} = \frac{\sigma_{yz}}{2G},$$

$$\varepsilon_{zx} = \frac{\sigma_{zx}}{2G} \tag{5}$$

where $\tau = T\text{-}T_0$ is the temperature variation of the object and α is the thermal expansion coefficient. Equation (5) can also be expressed as follows:

$$\sigma_{xx} = 2G\varepsilon_{xx} + \lambda\theta - \frac{\alpha ET}{1-2\nu},$$

$$\sigma_{xy} = 2G\varepsilon_{xy}$$

$$\sigma_{yy} = 2G\varepsilon_{yy} + \lambda\theta - \frac{\alpha ET}{1-2\nu},$$

$$\sigma_{yz} = 2G\varepsilon_{yz}$$

$$\sigma_{zz} = 2G\varepsilon_{zz} + \lambda\theta - \frac{\alpha ET}{1-2\nu},$$

$$\sigma_{zx} = 2G\varepsilon_{zx} \tag{6}$$

where E is the elastic modulus, ν is Poisson ratio, $\theta = \varepsilon_{xx} + \varepsilon_{yy} + \varepsilon_{zz}$ is the volumetric strain, T is the temperature variation range, $G = E/(2\times(1+\nu))$ is the modulus of elasticity in shear, and $\lambda = \nu E/((1+\nu)\times(1-2\nu))$ is the Lame constant.

Table 1: The chemical composition of HT250 gray cast iron.

Elements	C	Si	Mn	P	S	Cu	Cr	Fe
Composition (wt.%)	3.25	1.57	0.92	0.06	0.059	0.50	0.27	Bal.

Table 2: Thermal/physical properties of GCI and EN1A tool steel.

Thermal/physical parameter	GCI	EN1A Steel
Thermal conductivity, K_e/[W/(m · K)]	48	32.2
Density, ρ/(kg/m^3)	7200	7800
Specific heat capacity, c/[J/(kg · K)]	480	460
Thermal expansion coefficient, α/($\times 10^{-5}$K^{-1})	1.2	0.91
Elastic modulus, E/Gpa	120	210
Poisson ratio, ν	0.25	0.30

2.2. Modelling and Testing Procedure. The dimensions of the finite element (FE) model, established according to the actual pin-on-disc friction system, are as follows: outer diameter of Φ 54mm and inner diameter of Φ 38mm, with the thickness of 10 mm (see Figure 2). The material of the disc is GCI, codenamed HT250 (ISO 250), whose chemical composition is listed in Table 1, and its microstructure is displayed in Figure 3(a). The pin diameter is Φ 4.8 mm × 12.7 mm, manufactured from EN1A steel. The thermal physical properties of GCI and EN1A steel are both listed in Table 2. The main parameters of the pits include diameter of the pit, DOP, and distance between pits, DBP. In order to reveal the thermal behavior of different samples intuitively and visually, node 1 (see Figure 2) was introduced and used to reflect the thermal stress and temperature variation in simulation. The distance between node 1 and the upper surface of the sample is 1.0 mm, which is equal to the depth of the pits.

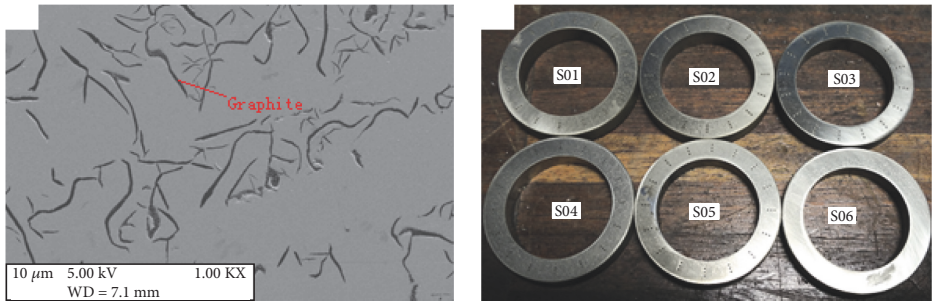

(a) (b)

Figure 3: SEM photo of GCI and the photo of samples. (a) SEM photo of GCI; (b) photo of S01-S06.

Table 3: The parameters of different samples S01-S06.

Sample No.	Diameter of pit, DOP (mm)	Distance between pits, DBP (mm)
S01	0.8	1.00
S02	0.8	1.25
S03	0.8	1.50
S04	0.4	1.00
S05	0.6	1.00
S06	-	-

A laser marking system (CL-FLS-30W, Shenyang Qianshi Laser CO., LTD.) was used to process the pits on the surface of the GCI discs. The laser processing parameters were as follows: 1064 nm wavelength, laser power, 30 W, diameter of laser beam, 0.05 mm, and scanning speed, 5 mm/s. As shown in Table 3, there were six samples fabricated in all. To imitate the head surface of a dung beetle, the samples with 16 sets of pits along the radial direction were called 'nonsmooth' samples and named from S01 to S05 according to the pit parameters. The other sample with a polished surface was introduced for comparison and called the "smooth" sample and marked as S06. Figure 3(b) shows the photo of all those samples.

Wear tests were conducted using a tribology wear testing rig (courtesy of the Surface Engineering Group, Manchester Metropolitan University, MMU) under dry sliding condition, with a normal load of 70 N, equivalent to a pressure of approximately 0.98 MPa, at room temperature, 20°C. The relative rotation speed was 200 rpm, equivalent to 21 rad s^{-1} (about 0.966 m/s at the centre of the pin), and the duration of the tests was designated as 500 seconds. To ensure the accuracy of the result, friction and wear tests were repeated 3 times for each specimen. Prior to the wear tests, the specimens and self-designed counterface (EN1A steel, with a hardness of approximately 800 HV) were mechanically polished with SiC papers (from No. 200 to No. 2000), followed by ultrasonic cleaning in acetone. Before and after testing, samples were cleaned and weighed by an electronic balance (Ohaus T2914) with a precision of 0.1 mg. The wear resistance of the specimens was measured and evaluated by its mass loss, which was the average of three measurements. The worn surfaces were observed by optical microscopy (S1000 Industrial Stereo Microscope, Spectrographic Limited, with Vimage software of Suzhou Vezu Opto Technology, CO., LTD.). The average surface hardness and roughness of GCI samples were 0.111 μm and 122.4 $HV_{0.5}$, respectively, obtained by THV-5 vickers hardness tester and TR300 roughness profile rig (TIME3230 module).

3. Tribological Behavior of Pit Textured Surfaces

3.1. Simulation Results. Based on the mechanical and thermodynamic models in the documents [17, 18], the FE model was established by APDL programming through an ANSYS/LS-DYNA module. The surface between the pit textured disc and the pin was set as a friction pair, wherein the upper surface of the disc was the target surface and the lower surface of the column pin was the contact surface. During the simulation process, the friction pair are always kept in contact with each other under a pressure of 0.98 MPa. To intuitively display the relative positions of disc and pin, based on the equivalent principle, the disc was constricted in all DOFs instead of the pin, as shown in Figure 2, and kept motionless in the simulation. An angular velocity, 21 rad/s (in the anticlockwise direction, about 200 RPM), was applied to the pin, which could rotate counterclockwise. The duration of the simulation is 0.5 s (100 substeps, i.e., 0.005 second per substep); thus, only heat conduction of the friction interface was considered in the simulation. The element type used in this work includes SOLID226, TARGE170, CONTA174, and MPC184. The number of elements is 32951 (S01).

Figure 4 shows the temperature-time curves of node 1 of S01-S06. It is evident that (1) there were three temperature peaks for all curves, which was consistent with the rotated times of the pin; (2) for S01-S03, their temperature curves were almost the same, with the lowest average temperature; (3) the average temperature of S04 was the highest among S01-S06, followed by S05; (4) the average temperature of S06 was higher than S01-S03, but lower than S04-S05.

Figure 5 exhibits the temperature contours of S01-S06 at the 0.5 s. The term "SMX" in the figure refers to the maximum value of temperature. The following results can be obtained from the figure: (1) compared with the smooth surface, the pits had a significant influence on the temperature

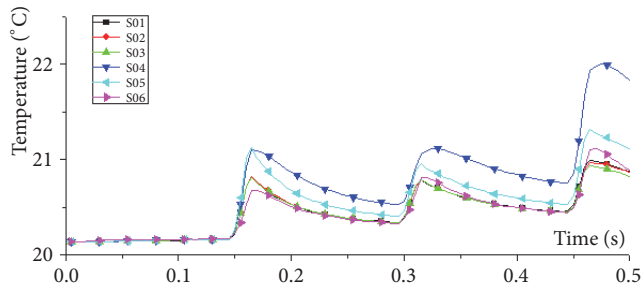

Figure 4: Temperature-time curves of node 1 of S01-S06.

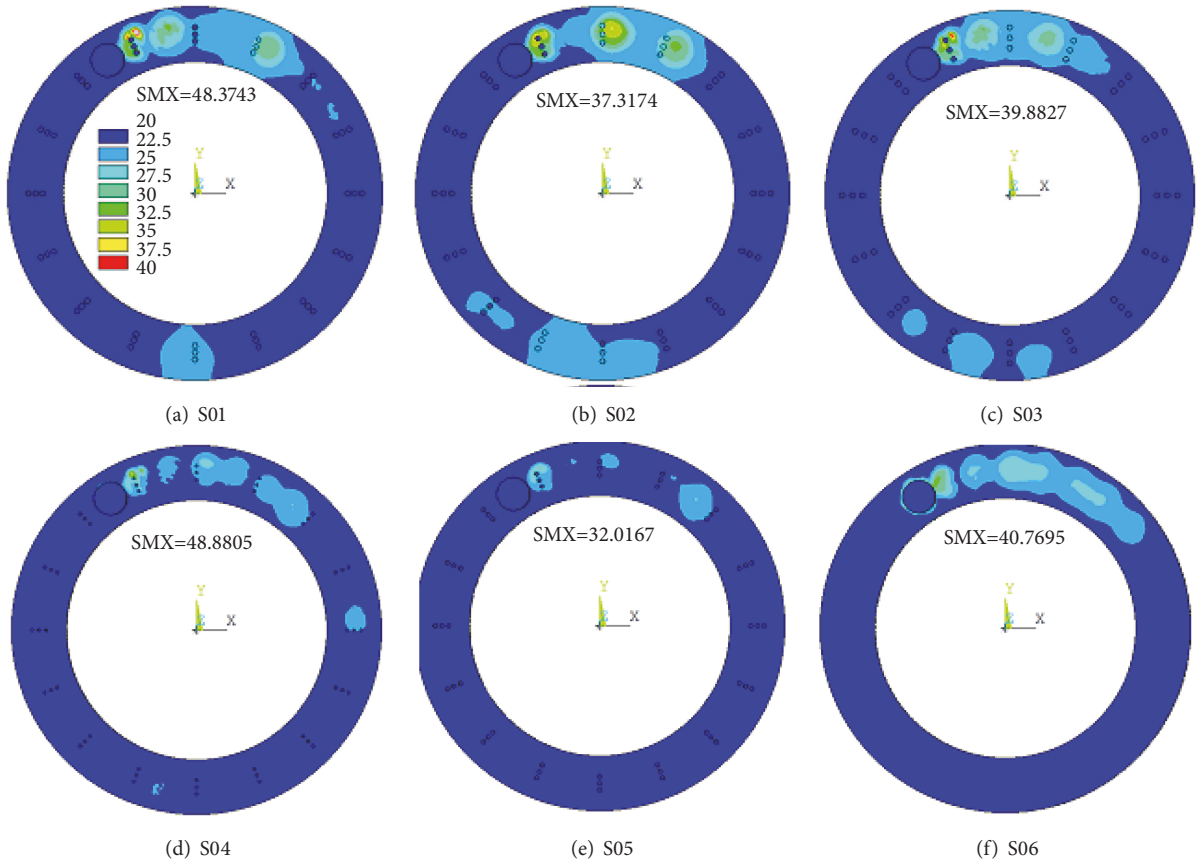

(a) S01 (b) S02 (c) S03

(d) S04 (e) S05 (f) S06

Figure 5: Temperature contours of S01-S06 at the 0.5 s.

distribution of the samples; (2) the heat affected area of S01 was the largest, while the high temperature area of S05 was the smallest; (3) for S01-S03, there were obvious high temperature regions near the pits, as well as the "temperature crawling" phenomena; (4) for S04 and S05, there was no evident temperature concentration or crawling phenomena on the surfaces; (5) the temperature distribution of S06 displayed a "long tail" along the rotating direction, without any "temperature crawling" phenomenon.

Figure 6 displays the *von Mises* stress contours of the samples at the 0.5 s. The term "SMX" in the figure refers to the maximum value of *von Mises* stress. It is obvious that (1) the pits can influence the *von Mises* stress distribution of the samples, especially at locations near the pits. There were obvious low *von Mises* stress areas near the pits along the rotating direction for all pit textured specimens; (2) among S01-S03, the *von Mises* stress affected area of S01 was the smallest; (3) the high *von Mises* stress areas of S04 and 05 were both larger than that of S01, with the high *von Mises* stress area of S05 being the largest; (4) evidently, the high *von Mises* stress distribution of S06 was smoother and more continuous.

3.2. Tribological Behavior. Figure 7 shows the friction coefficient curves and mass loss curve of samples S01-S06. It is clear to see that (1) among all the specimens, the friction coefficient and wear rate of S01 were the lowest, while the wear rate of S03 was the largest. The friction coefficient and wear loss rate of S06 were also quite low; (2) for S01-S03, the

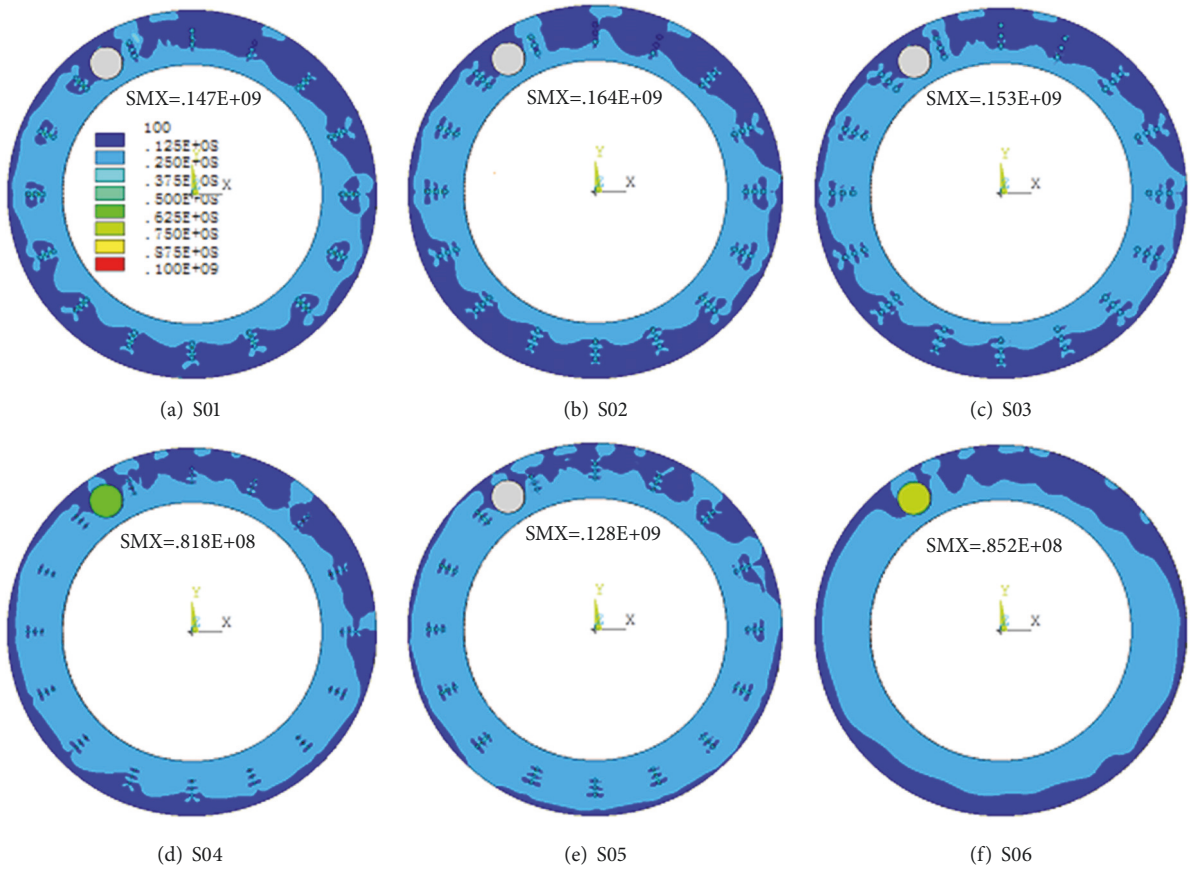

(a) S01 (b) S02 (c) S03

(d) S04 (e) S05 (f) S06

Figure 6: The *von Mises* equivalent stress contours of S01-S06 at the 0.5 s.

wear rate increased with the variation of DBP from 1.0 mm to 1.50 mm, while the friction coefficient increased first and then decreased; (3) for S04, S05, and S01, with the increase of DOP, the wear rate increased first and then decreased, but the friction coefficient kept increasing.

The worn surfaces of S01-S06 are shown in Figure 8. The surface conditions of the nonsmooth and smooth specimens are consistent with the results of Figure 7. It is also obvious that (1) there was only slight wear tracks on the surface of S01; (2) the wear of S03 was very serious, and there were very deep and continuous furrows (see the red circle of S03), indicating the poor antiwear performance; (3) for S02, S04-S06, there were obvious grinding phenomena on the surface (see the red circle regions of them), especially S02.

4. Discussion

For the pit textured surfaces, DOP and DBP are the key parameters which affect their final antiwear properties. When DOP was constant, as shown in Figure 8, the wear resistance of the pit textured samples gradually deteriorated with the increase of DBP from 1.0 mm to 1.50 mm. By comparing Figures 5 and 6, it is evident that increasing of DBP could significantly enlarge the heat affected zone and high thermal stress region of the textured surface, which was detrimental to obtaining good antiwear performance. In addition, increasing of DBP was also not conducive to the collection of debris during the dry wear process, which would cause a transition from "adhesive wear" to "three-body abrasion" and to, therefore, deteriorate the wear resistance of the pit textured surfaces. Conversely, when DBP remained constant, with an increase of DOP, the heat affected area gradually enlarged, but the high thermal stress region gradually reduced. Correspondingly, the friction coefficient and wear volume also decreased with the change of DOP from 0.4 mm to 0.8 mm. In general, the parameters of S01 are the best among all samples, i.e., DOP of 0.8 mm, and DBP of 1.0 mm, which are consistent with the results published previously [15, 16].

As shown in Figures 5 and 6, compared with the smooth sample, nonsmooth pit structures can clearly alter the thermal stress and temperature distribution of the textured surfaces, inducing extremely nonuniform thermal stresses and temperature fields, even causing a 'temperature crawling' phenomenon, which are disadvantageous factors for pit textured surfaces to achieve good antiwear properties. In the meantime, the pits in the nonsmooth samples can trap and hold the debris (see Figure 9) produced in the friction process under dry wear condition, which is an advantageous factor for pit textured surfaces to obtaining excellent wear resistance. The final influence of the pit textured surfaces on the wear resistance of nonsmooth specimens depends on the combined result of the two aspects mentioned above.

Furthermore, for the actual pin-on-disc friction system, the pin is fixed during the wear testing, and the disc rotates

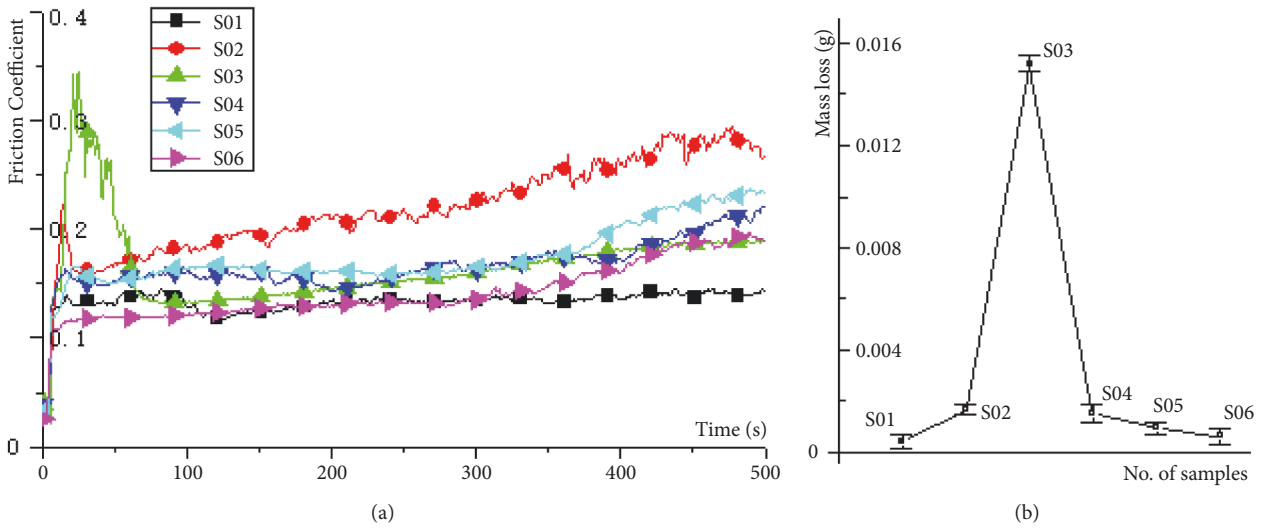

FIGURE 7: Friction coefficient curves and mass loss curve of S01-06. (a) Friction coefficient curves of S01-06; (b) mass loss curve of S01-06.

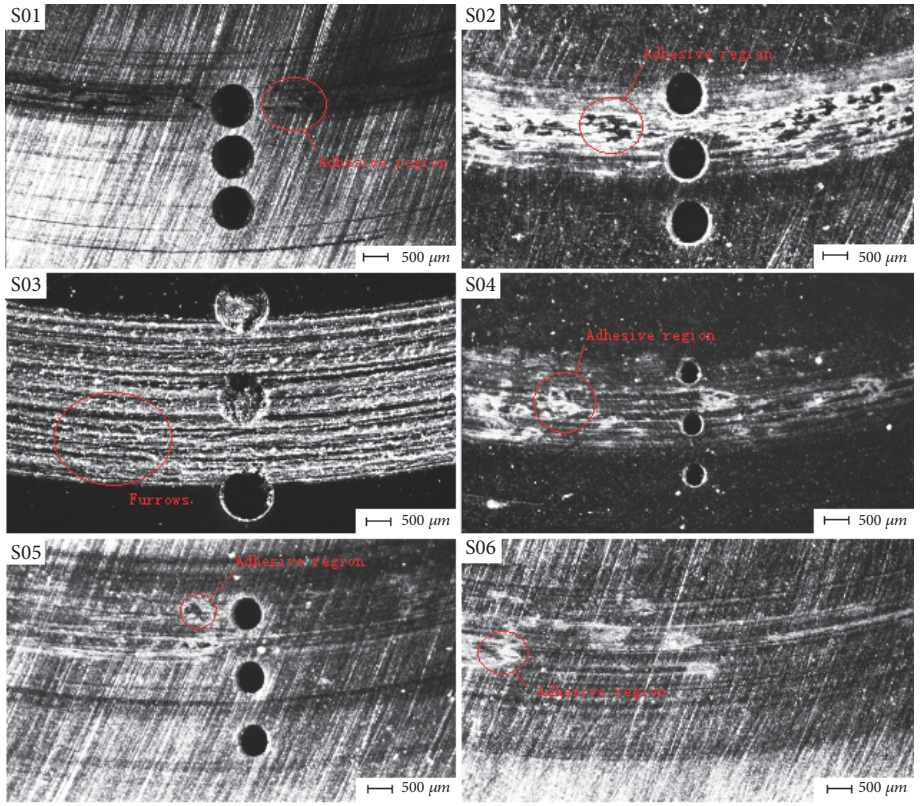

FIGURE 8: Worn surfaces of S01-S06 after wear testing.

anticlockwise or clockwise. The debris left on the textured surface will be subjected to the action of two kinds of forces; one is the pressure of the pin, and the other is the centrifugal force due to the rotation of the disc (see Figure 9). When the rotating speed is high enough, the centrifugal force may be greater than the pushing force of the pin; some debris may move inward firstly, and then move outward possibly. The change of the motion direction of the debris will cause a "secondary grinding phenomenon" on textured or smooth surfaces. This is the reason for the serious adhesive wear (see Figure 8) of the pit textured samples.

5. Conclusions

Through numerical simulation and experimental analysis, the influence of pit textured surfaces on the tribological

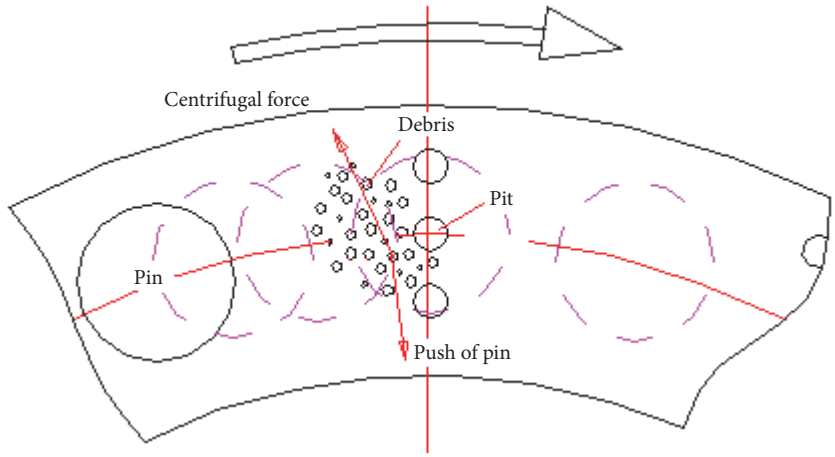

Figure 9: Influence mechanism of pit textured surface.

behavior of a pin-on-disc system was investigated and reported in this work. An underlying mechanism was also proposed and discussed, and the following conclusions could be drawn.

(1) DOP and DBP are two important parameters that affect the wear resistance of pit textured surfaces. The simulated data shows that pits can significantly change the thermal stress and temperature distribution of the textured surfaces during friction and wear processes and result in low thermal stress zones near the dimples. In addition, when the DOP is 0.8 mm, there are obvious 'temperature crawling' phenomena on the pit textured surfaces.

(2) Compared with the smooth sample, the pit textured structure is able to either improve or worsen the surface abrasion resistance of the specimen, depending on the combined effect of the capacity of the pits to contain debris and the ability of the pits to change the thermal stress and temperature distribution of the textured surface. According to the above results, when DOP is 0.8 mm and DBP is 1 mm, the pit textured surface has the best wear resistance under dry friction conditions.

The influence of other texture patterns (streaks, rectangles, diamonds, and their combinations) on the tribological behavior will also be reported and shared in the future.

Data Availability

The original codes and data used to support the findings of this study are available from the corresponding author upon request.

Conflicts of Interest

The authors declare that there are no conflicts of interest regarding the publication of this paper.

Acknowledgments

The research is supported by China Scholarship Council, as well as the 2014 Shanxi coal-based key scientific & technological projects (MJ2014-06). Besides the Shanxi Key Laboratory of Fully Mechanized Coal Mining Equipment, China, the authors would like to thank the coworkers of MMU.

References

[1] N. Sun, H. Shan, H. Zhou et al., "Friction and wear behaviors of compacted graphite iron with different biomimetic units fabricated by laser cladding," *Applied Surface Science*, vol. 258, no. 19, pp. 7699–7706, 2012.

[2] G. Ryk, Y. Kligerman, and I. Etsion, "Experimental investigation of laser surface texturing for reciprocating automotive components," *Tribology Transactions*, vol. 45, no. 4, pp. 444–449, 2002.

[3] I. Etsion, "State of the art in laser surface texturing," *Journal of Tribology*, vol. 127, no. 1, pp. 248–253, 2005.

[4] Y. Wan and D.-S. Xiong, "Study of laser surface texturing for improving tribological properties," *Mocaxue Xuebao/Tribology*, vol. 26, no. 6, pp. 603–607, 2006.

[5] H. Zhou, X. Tong, Z. Zhang, X. Li, and L. Ren, "The thermal fatigue resistance of cast iron with biomimetic non-smooth surface processed by laser with different parameters," *Materials Science and Engineering: A Structural Materials: Properties, Microstructure and Processing*, vol. 428, no. 1-2, pp. 141–147, 2006.

[6] X. Tong, H. Zhou, Z.-H. Zhang, N. Sun, H.-Y. Shan, and L.-Q. Ren, "Effects of surface shape on thermal fatigue resistance of biomimetic non-smooth cast iron," *Materials Science and Engineering: A Structural Materials: Properties, Microstructure and Processing*, vol. 467, no. 1-2, pp. 97–103, 2007.

[7] X. Tong, H. Zhou, M. Liu, and M.-J. Dai, "Effects of striated laser tracks on thermal fatigue resistance of cast iron samples with biomimetic non-smooth surface," *Materials and Corrosion*, vol. 32, no. 2, pp. 796–802, 2011.

[8] Z. Jing, H. Zhou, P. Zhang, C. Wang, C. Meng, and D. Cong, "Effect of thermal fatigue on the wear resistance of graphite cast iron with bionic units processed by laser cladding WC," *Applied Surface Science*, vol. 271, pp. 329–336, 2013.

[9] B. Kim, Y. H. Chae, and H. S. Choi, "Effects of surface texturing on the frictional behavior of cast iron surfaces," *Tribology International*, vol. 70, pp. 128–135, 2014.

[10] D. Braun, C. Greiner, J. Schneider, and P. Gumbsch, "Efficiency of laser surface texturing in the reduction of friction under mixed lubrication," *Tribology International*, vol. 77, pp. 142–147, 2014.

[11] R. Bathe, V. Sai Krishna, S. K. Nikumb, and G. Padmanabham, "Laser surface texturing of gray cast iron for improving tribological behavior," *Applied Physics A: Materials Science & Processing*, vol. 117, no. 1, pp. 117–123, 2014.

[12] X. Yao, H. Huo, M. Bao, and L. Tian, "Impact fatigue behavior of ZrN/Zr-N/Zr coatings on H13 steel by CFUBMSIP," *Journal of Wuhan University of Technology-Mater. Sci. Ed.*, vol. 29, no. 1, pp. 137–142, 2014.

[13] Z.-K. Chen, S.-C. Lu, X.-B. Song, H. Zhang, W.-S. Yang, and H. Zhou, "Effects of bionic units on the fatigue wear of gray cast iron surface with different shapes and distributions," *Optics & Laser Technology*, vol. 66, pp. 166–174, 2014.

[14] L. Zheng, J. Wu, S. Zhang et al., "Bionic Coupling of Hardness Gradient to Surface Texture for Improved Anti-wear Properties," *Journal of Bionic Engineering*, vol. 13, no. 3, pp. 406–415, 2016.

[15] S.-N. Sun, L.-Y. Xie, and Y.-C. Zhang, "Finite element analysis on friction and wear properties of non-smooth surface brake disc," *Dongbei Daxue Xuebao*, vol. 35, no. 11, pp. 1597–1601, 2014.

[16] S. Sun, L. Xie, P. Kelly, R. Long, M. Li, and J. Feng, "The Influence of Rotating Direction on the Tribological Behavior of Grey Cast Iron with Curve Distributed Pit Textured Surface," *Mathematical Problems in Engineering*, vol. 2017, Article ID 8095916, 10 pages, 2017.

[17] L. Ri-Sheng, S. Shao-Ni, and L. Zi-Sheng, "The influence of scanning methods on the cracking failure of thin-wall metal parts fabricated by laser direct deposition shaping," *Engineering Failure Analysis*, vol. 59, pp. 269–278, 2016.

[18] R. Long, S. Sun, and Z. Lian, "Research on the Hard-Rock Breaking Mechanism of Hydraulic Drilling Impact Tunneling," *Mathematical Problems in Engineering*, vol. 2015, Article ID 153648, 34 pages, 2015.